

# Rotation and anisotropy of galaxies revisited

James Binney

*Rudolf Peierls Centre for Theoretical Physics, Keble Road, Oxford OX1 3NP*

## ABSTRACT

The use of the tensor virial theorem (TVT) as a diagnostic of anisotropic velocity distributions in galaxies is revisited. The TVT provides a rigorous global link between velocity anisotropy, rotation and shape, but the quantities appearing in it are not easily estimated observationally. Traditionally use has been made of a centrally averaged velocity dispersion and the peak rotation velocity. Although this procedure cannot be rigorously justified, tests on model galaxies show that it works surprisingly well. With the advent of integral-field spectroscopy it is now possible to establish a rigorous connection between the TVT and observations. The TVT is reformulated in terms of sky-averages, and the new formulation is tested on model galaxies.

**Key words:** galaxies: kinematics and dynamics

## 1 INTRODUCTION

Thirty years ago our understanding of elliptical galaxies was revolutionized by the discovery that most giant elliptical galaxies are not flattened by rotation (Bertola & Capaccioli 1977; Illingworth 1977; Binney 1978). Subsequently it emerged that a galaxy’s peak rotation speed is correlated with its luminosity, and the cusps and diskiness of its luminosity density: less luminous galaxies tend to have cuspiers central density profiles, disk rather than boxy isophotes, and a higher degree of rotational flattening than more luminous galaxies (Bender 1988; Kormendy & Bender 1996).

It is generally recognized that these correlations must be clues to how elliptical galaxies formed. A promising conjecture is that the current configuration of a boxy galaxy was largely established by a violent merger of galaxies of comparable mass, while cuspy galaxies were configured by a succession of minor mergers with companions substantially less massive than themselves (Naab, Burkert & Hernquist 1999; Naab & Burkert 2002). To assess the truth of this and any competing conjecture, we clearly need to characterize as fully as possible the degree of rotational flattening of any given galaxy, and to understand the significance of rotational flattening for the system’s internal dynamics.

Ideally one would explore the connections between diskiness, cusps and anisotropy by experimenting with a series of semi-analytic galaxy models that would be generalizations of popular spherical models (e.g., King 1966; Jaffe 1983; Hernquist 1990). Unfortunately, even now the repertoire of semi-analytic flattened models is very sparse, and all of these models are unrealistic in one significant respect or another. Moreover, thirty years ago, when the importance of anisotropy was first realized, even fewer semi-analytic models were available, and our theoretical

understanding has relied heavily on (a) N-body models (Binney 1976; Aarseth & Binney 1978; Barnes & Hernquist 1992), (b) Schwarzschild modelling (Schwarzschild 1979; Levison & Richstone 1980), and (c) the tensor virial theorem (Binney 1978).

The tensor virial theorem (TVT) provides a powerful general framework within which to discuss the connection between rotation and flattening, but it is not straightforward to connect the quantities that appear in it to observable quantities. Until recently it was in principle impossible to make this connection rigorously because the TVT operates at a global level, while galaxy kinematics could be probed only along a limited number of slits, that rarely extended very far out in the galaxy, especially perpendicular to the apparent major axis. With the advent of integral-field spectroscopy (Bacon et al. 2002; de Zeeuw et al. 2002; Kelz, Roth & Becker 2003) this problem is substantially alleviated, and it is now time to reassess how the TVT is used to interpret kinematic data. This task is the primary goal of this paper. In the process we make a critical reassessment of how traditional long-slit data are interpreted.

## 2 THE TENSOR VIRIAL THEOREM

The TVT states that in any equilibrium stellar system (Chandrasekhar 1969; Binney & Tremaine 1987)

$$2\mathbf{K} + \mathbf{W} = 0, \tag{1}$$

where the kinetic- and potential-energy tensors are

$$K_{ij} \equiv \frac{1}{2} \int d^6\mathbf{w} v_i v_j f(\mathbf{w})$$

$$W_{ij} \equiv - \int d^3 \mathbf{x} \rho x_i \frac{\partial \Phi}{\partial x_j}. \quad (2)$$

Here  $\mathbf{w} \equiv (\mathbf{x}, \mathbf{v})$  is the vector of phase-space coordinates,  $f$  is the system's distribution function,  $\rho(\mathbf{x}) \equiv \int d^3 \mathbf{v} f(\mathbf{w})$  is the density, and  $\Phi(\mathbf{x})$  is the gravitational potential.  $\mathbf{K}$  is customarily decomposed into contributions from ordered and random motion

$$\mathbf{K} = \mathbf{T} + \frac{1}{2} \mathbf{\Pi}, \quad (3)$$

where

$$T_{ij} \equiv \frac{1}{2} \int d^3 \mathbf{x} \bar{v}_i \bar{v}_j \rho$$

$$\Pi_{ij} \equiv \int d^6 \mathbf{w} (v_i - \bar{v}_i)(v_j - \bar{v}_j) f(\mathbf{w}). \quad (4)$$

Here a bar over any quantity denotes an average over velocity space:

$$\bar{v}_i(\mathbf{x}) \equiv \frac{1}{\rho(\mathbf{x})} \int d^3 \mathbf{v} v_i f(\mathbf{w}). \quad (5)$$

We use this notation to define the velocity-dispersion tensor

$$\sigma_{ij}^2 \equiv \overline{(v_i - \bar{v}_i)(v_j - \bar{v}_j)}. \quad (6)$$

In the case of a flattened, axisymmetric galaxy, we expect the principal axes of the tensors above to coincide with the symmetry axis, which we label the  $z$  axis, and any two perpendicular axes – the  $x$  and  $y$  axes. Then  $\mathbf{\Pi}$  can be characterized by two numbers:  $\sigma_0^2$  and the global anisotropy parameter  $\delta$ , which are defined such that

$$\Pi_{xx} = M\sigma_0^2 \quad ; \quad \Pi_{zz} = (1 - \delta)M\sigma_0^2, \quad (7)$$

where  $M$  is the galaxy's mass. If we assume that the galaxy's only streaming motion is rotation, we may characterize  $\mathbf{T}$  by a single number  $v_0$  through

$$T_{xx} = T_{yy} = \frac{1}{4} M v_0^2, \quad (8)$$

where the factor  $\frac{1}{4}$  is chosen so that the total ordered kinetic energy is  $T_{xx} + T_{yy} = \frac{1}{2} M v_0^2$ . With this notation it is easy to show that the TVT (1) implies that (Binney 1978)

$$\frac{v_0^2}{\sigma_0^2} = 2(1 - \delta) \frac{W_{xx}}{W_{zz}} - 2. \quad (9)$$

In the case that the galaxy's surfaces of constant density are all similar spheroids of axis ratio  $1 - \epsilon$ , the ratio  $W_{xx}/W_{zz}$  on the right of this equation is a function of  $\epsilon$  and independent on the galaxy's radial density profile (Roberts 1962), so this equation provides a connection between the rotation rate  $v_0$ , the mean-square velocity dispersion parallel to the equatorial plane  $\sigma_0^2$ , and the global anisotropy parameter  $\delta$ . If  $v_0$  and  $\sigma_0$  could be estimated from observational measurements of the line-of-sight mean velocity and velocity dispersion, equation (9) would enable one to determine the anisotropy parameter  $\delta$  from observational data.

### 3 APPLICATION TO TRADITIONAL DATA

Following Illingworth (1977) and Davies et al. (1983),  $\sigma_0$  has often been identified with  $\sigma_{0.5}$ , the mean velocity dispersion interior to  $\sim \frac{1}{2} R_e$ , while the peak line-of-sight streaming velocity  $v_{\max}$  is identified with  $\frac{1}{4} \pi v_0$ . There is no rigorous basis for either identification since both the velocity dispersion

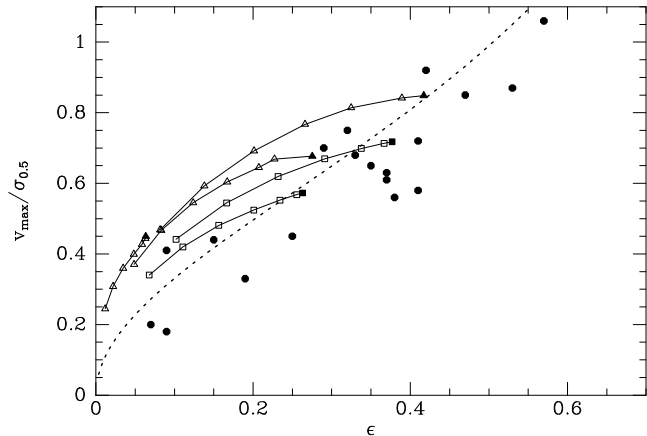


**Figure 1.** Squares: the ratio of peak line-of-sight streaming velocity to line-of-sight velocity dispersion for two Evans models. Triangles: the same data for three Rowley models. The point at the upper right of each chain is for an edge-on model, and successive points on the chain show the effect of reducing the inclination by  $10^\circ$ . The dashed curve shows the relation (9) between  $v_{\max} = \frac{1}{4} \pi v_0$  and  $\sigma_0$  for  $\delta = 0$ . The circles show observed values of  $v_{\max}/\sigma_{0.5}$  for spheroids less luminous than  $M_B = -20.5$ .

and the streaming velocity are expected to depend on the location of the line-of-sight. The factor  $\frac{1}{4} \pi$  is motivated by the consideration that if the luminosity density  $j(R, z)$  scales with galactocentric distance  $(R^2 + z^2)^{-3/2}$ , and the streaming velocity is independent of  $R$ , then when the galaxy is viewed edge-on, the line-of-sight streaming velocity will be a factor  $\pi/4$  smaller than the three-dimensional streaming velocity (Binney 1978).

We can test the reliability of these traditional identifications by applying them to models that have analytic distribution functions of the form  $f(E, L_z)$  and self-consistent gravitational potentials, where  $E$  and  $L_z$  are respectively the stellar energy and angular momentum about the symmetry axis. Fig. 1 shows data for two types of semi-analytic model.

#### 3.1 Evans models

Evans (1994) presented a family of models, called ‘power-law models’, in which the potential varies as a power of the spheroidal variable  $m = \sqrt{R_c^2 + R^2 + z^2/q_\Phi^2}$ . Here  $R_c$  is a constant that sets the linear scale of the model, while  $q_\Phi$  determines the model's flattening. The index  $y$  in the power-law relation  $\Phi \propto (R_c^2/m^2)^y$  determines the asymptotic slope of the circular-speed curve – the models shown in Fig. 1 both have  $y = 0.09$ , which corresponds to a gently falling asymptotic circular-speed curve.

The part  $f_+(E, L_z)$  of the distribution function that is even in  $L_z$  is uniquely determined by Poisson's equation, and we define the odd function  $f_-(E, L_z)$  to be equal to  $f_+(E, L_z)$  for  $L_z > 0$ . The complete distribution function is taken to be  $f = f_+ + \gamma f_-$ . With this choice of distribution function, the streaming velocity at any point in the model is proportional to  $\gamma$  and we choose  $\gamma$  as the average of the individual values that would make  $\sigma_\phi = \sigma_R$  at a grid of points in the equatorial plane. That is,  $\gamma$  is chosen to make the model as near as possible an isotropic rotator.

The squares in Fig. 1 show centrally averaged line-of-sight velocity dispersion and  $v_{\max}$  for Evans models with  $q_{\Phi} = 0.85$  and  $q_{\Phi} = 0.9$ . The value of  $\epsilon$  is for the isophote with semi-major axis length  $15R_c$ , and  $\sigma_{0.5}$  is the mean value of the line-of-sight velocity dispersion on the major axis out to  $15R_c$ . The filled squares are for a model seen edge-on, while successive open squares show data for the models seen at inclination  $i = 80^\circ, 70^\circ, \dots$

### 3.2 Rowley models

Rowley (1988) developed models of flattened stellar systems to use as model bulges. These systems are defined by their distribution function

$$f \propto \begin{cases} e^{\chi/\sigma^2} & \text{for } \chi > 0, \\ 0 & \text{otherwise,} \end{cases} \quad (10)$$

where

$$\chi = \chi_0 - E + \omega L_z - \frac{1}{2} L_z^2 / r_a^2, \quad (11)$$

with  $E$  stellar energy,  $L_z$  angular momentum about the symmetry axis, and  $\sigma$ ,  $\chi_0$ ,  $\omega$  and  $r_a$  being constants. It is easy to show that  $\chi$  can be rewritten as

$$\chi = \Psi - \frac{1}{2} v_m^2 - \frac{1}{2} \left( 1 + \frac{R^2}{r_a^2} \right) \left( v_{\phi} - \frac{\omega R}{1 + R^2/r_a^2} \right)^2, \quad (12)$$

where  $v_m$  is the speed in the meridional plane, and

$$\Psi \equiv \chi_0 - \Phi + \frac{\omega^2 R^2}{2(1 + R^2/r_a^2)}. \quad (13)$$

From equations (10) and (12) we can identify the streaming velocity

$$\bar{v}_{\phi} = \frac{\omega R}{1 + R^2/r_a^2}, \quad (14)$$

and observe that the distribution of stellar velocities is a truncated bi-axial Gaussian around  $\bar{v}_{\phi}$ . We see also that the density vanishes for  $\Psi \leq 0$ . We define the tidal radius  $R_t$  as the radius at which this inequality is first satisfied in the equatorial plane. Rowley models are characterized by the dimensionless spin parameter  $\omega r_a / \sigma^2$  and the dimensionless potential difference  $\Delta = [\Psi(0, 0) - \Psi(R_t, 0)] / \sigma^2$ .

Each filled triangle in Fig. 1 shows the ratio of  $v_{\max}$  to centrally-averaged velocity dispersion versus the ellipticity of the isophote at  $3R_e$  for a Rowley model seen edge-on, while the open triangles show the corresponding data for the models seen at inclinations  $i = 80^\circ, 70^\circ, \dots$ . All models have  $\Delta = 4$ , and  $\omega r_a / \sigma = 0.9, 1.35, 1.69$  for the three models.

We see that at a given ellipticity, Rowley models rotate more rapidly than Evans models. This phenomenon reflects the low ratio of  $\sigma_{\phi}$  to  $\sigma_R$  that follows from equation (12). When a razor-thin disk is added to a model, the flattening of the system is increased while its rotation stays the same, and for realistic parameters the system can move into the band in the  $(v/\sigma, \epsilon)$  plane that is occupied by bulges (Rowley 1988).

The dashed curve in Fig. 1 shows the relation between  $\frac{1}{4}\pi v_0/\sigma_0$  and  $\epsilon$  that is predicted by equation (9). The curve runs close to the location of edge-on Evans models, which are very nearly isotropic rotators, while the Rowley models, which are slightly anisotropic in the sense that  $\sigma_{\phi}^2 < \sigma_R^2 = \sigma_z^2$ , lie above the dashed curve. Thus Fig. 1

validates the traditional use of the TVT to draw the trajectory of isotropic rotators in the  $(v/\sigma, \epsilon)$  plane. The models demonstrate that tilting a galaxy away from edge-on orientation tends to push its representative point above the dashed curve. Hence galaxies that lie well below this curve, as luminous elliptical galaxies nearly all do, must certainly be anisotropic in the sense of having larger pressure parallel to the equatorial plane than perpendicular to it.

In Fig. 1 circles show ratios of peak rotation speed to velocity dispersion averaged within  $\frac{1}{2}R_e$  for real spheroidal systems less luminous than  $M_B = -20.5$  (for  $H_0 = 50 \text{ km s}^{-1} \text{ Mpc}^{-1}$ ) from Davies et al. (1983). These circles straddle the dashed curve, with rather more points below than above it, suggesting that these systems are at most mildly anisotropic.

## 4 APPLICATION TO MODERN DATA

Observers measure the line-of-sight velocity distribution (LOSVD)

$$F(\mathbf{x}_{\perp}, v_{\parallel}) = \frac{1}{\Sigma(\mathbf{x}_{\perp})} \int d\mathbf{x}_{\parallel} \int d^2\mathbf{v}_{\perp} f(\mathbf{w}), \quad (15)$$

where

$$\Sigma \equiv \int d\mathbf{x}_{\parallel} \rho(\mathbf{x}) \quad (16)$$

is the surface density and the subscripts  $\parallel$  and  $\perp$  respectively denote components of vectors parallel and perpendicular to the line of sight. They quantify  $F$  by the moments

$$\sigma_{\parallel}^2(\mathbf{x}_{\perp}) = \int dv_{\parallel} (v_{\parallel} - \tilde{v}_{\parallel})^2 F(\mathbf{x}_{\perp}, v_{\parallel}) \quad (17)$$

and  $\tilde{v}_{\parallel}(\mathbf{x}_{\perp})$ , where we have introduced the notation that for any function  $g(v_{\parallel})$ ,

$$\begin{aligned} \tilde{g}_{\parallel}(\mathbf{x}_{\perp}) &\equiv \int dv_{\parallel} g(v_{\parallel}) F(\mathbf{x}_{\perp}, v_{\parallel}) \\ &= \frac{1}{\Sigma} \int d\mathbf{x}_{\parallel} \int d^3\mathbf{v} g(v_{\parallel}) f(\mathbf{w}). \end{aligned} \quad (18)$$

Integral-field spectrographs such as SAURON (de Zeeuw et al. 2002) enable one to map  $\tilde{v}_{\parallel}$  and  $\sigma_{\parallel}^2$  over a significant part of the galaxy image. From such maps it is possible to measure quantities that are more directly related to the TVT than the quantities  $v_{\max}$  and  $\sigma_{0.5}$  defined above.

First we note that

$$\sigma_{\parallel}^2 = \tilde{v}_{\parallel}^2 - \tilde{v}_{\parallel}^2. \quad (19)$$

Using this relation to integrate  $\Sigma \tilde{v}_{\parallel}^2$  over the sky, we obtain

$$\begin{aligned} \int d^2\mathbf{x}_{\perp} (\sigma_{\parallel}^2 + \tilde{v}_{\parallel}^2) \Sigma &= \int d^3\mathbf{x} \int d^3\mathbf{v} v_{\parallel}^2 f(\mathbf{w}) \\ &= 2\hat{\mathbf{s}} \cdot \mathbf{K} \cdot \hat{\mathbf{s}}, \end{aligned} \quad (20)$$

where  $\hat{\mathbf{s}}$  is the unit vector parallel to the line of sight.

For  $\hat{\mathbf{s}}$  parallel to the  $x$  axis we can write this equation more compactly as

$$(\langle \sigma_{\parallel}^2 \rangle + \langle \tilde{v}_{\parallel}^2 \rangle) M = 2K_{xx}, \quad (21)$$

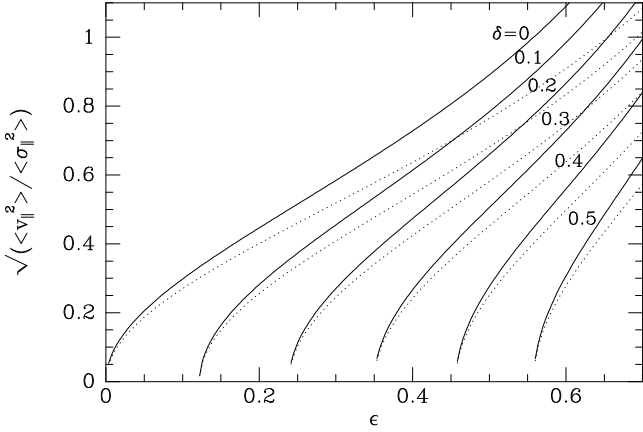


**Figure 2.** Modified TVT. The full curves show the relation between  $\langle \tilde{v}_{\parallel}^2 \rangle / \langle \sigma_{\parallel}^2 \rangle$  established by equation (26) when  $\alpha = 0$ , while the dotted curves show the relation when  $\alpha = 0.2$ .

where we have introduced the notation that with  $q(\mathbf{x}_{\perp})$  an arbitrary function on the sky, its sky-average is

$$\langle q \rangle \equiv \frac{1}{M} \int d^2 \mathbf{x}_{\perp} q \Sigma. \quad (22)$$

Equation (21) for  $K_{xx}$  enables us to derive from the  $xx$  and  $zz$  components of the TVT

$$M \frac{\langle \sigma_{\parallel}^2 \rangle + \langle \tilde{v}_{\parallel}^2 \rangle}{\Pi_{zz}} = \frac{W_{xx}}{W_{zz}}. \quad (23)$$

At any point  $\mathbf{x}$  in the galaxy let  $u(\mathbf{x})$  be the difference between the component  $\tilde{v}_{\parallel}$  of the streaming velocity parallel to the line of sight and the mean velocity for that line of sight,  $\tilde{v}_{\parallel}$ . With this definition,  $u \equiv \tilde{v}_{\parallel} - \tilde{v}_{\parallel}$ , it is easy to show that

$$\Sigma \sigma_{\parallel}^2 = \int dx_{\parallel} (\sigma_{xx}^2 + u^2) \rho(\mathbf{x}), \quad (24)$$

where  $\sigma_{xx}$  is defined by equation (6). Integrating this expression over the sky, we obtain

$$\Pi_{xx} = M \langle \sigma_{\parallel}^2 \rangle - \int d^3 \mathbf{x} u^2(\mathbf{x}) \rho(\mathbf{x}). \quad (25)$$

Finally we use this equation and equation (7) to eliminate  $\Pi_{zz}$  from equation (23), and obtain after some rearrangement

$$\frac{\langle \tilde{v}_{\parallel}^2 \rangle}{\langle \sigma_{\parallel}^2 \rangle} = \frac{(1 - \delta) W_{xx} / W_{zz} - 1}{\alpha (1 - \delta) W_{xx} / W_{zz} + 1}, \quad (26)$$

where

$$\alpha \equiv \frac{1}{M \langle \tilde{v}_{\parallel}^2 \rangle} \int d^3 \mathbf{x} u^2 \rho(\mathbf{x}). \quad (27)$$

In this form of the TVT, the left side contains only observationally accessible quantities, while the right side contains the standard global anisotropy parameter  $\delta$ , the shape parameter  $W_{xx}/W_{zz}$ , and a new dimensionless parameter  $\alpha$ , which quantifies the contribution of streaming motion to the line-of-sight velocity dispersion.

The value of  $\alpha$  depends on the shape of the galaxy's intrinsic rotation curve, and its radial luminosity profile, but not on the amplitude of the rotation curve. One may

straightforwardly show that it vanishes in the case of solid-body rotation, and increases with the shear of the stellar flow. For a fixed rotation curve, it is larger for flatter slopes of the radial luminosity density profile. A numerical calculation for the case of a galaxy in which the luminosity density follows the Hernquist (1990) profile shows that  $\alpha = 0.131$  if  $\bar{v}_{\phi} = \text{constant}$ .

Fig. 2 shows  $v/\sigma$  as a function of  $\epsilon$  from equation (26) for several values of  $\delta$  and two values of  $\alpha$ :  $\alpha = 0$  (full curves) and  $\alpha = 0.2$  (dotted curves). When  $\alpha = 0$  the right side of equation (26) becomes precisely half of the right side of the classical result (9). The factor half arises because in equation (9)  $v_0$  is a three-dimensional streaming velocity, whereas in equation (26)  $\sqrt{\langle \tilde{v}_{\parallel}^2 \rangle}$  is a projected velocity.

Probably equation (26) is most usefully recast as an expression for the anisotropy parameter  $\delta$  as a function of  $\alpha$ ,  $\epsilon$  and  $\langle \tilde{v}_{\parallel}^2 \rangle / \langle \sigma_{\parallel}^2 \rangle$ :

$$\delta = 1 - \frac{1 + \langle \tilde{v}_{\parallel}^2 \rangle / \langle \sigma_{\parallel}^2 \rangle}{1 - \alpha \langle \tilde{v}_{\parallel}^2 \rangle / \langle \sigma_{\parallel}^2 \rangle} \left( \frac{W_{zz}}{W_{xx}} \right). \quad (28)$$

#### 4.1 Practical considerations

Three issues arise when using observational data to evaluate the right side of equation (28). We cannot directly measure  $\alpha$ , but we can infer its value with reasonable accuracy from the shape of the measured rotation curve. In the tests below, I simply use the values directly calculated from the models. The second issue is that our kinematic data do not extend to arbitrary radii, so it is not practicable to evaluate the means  $\langle \tilde{v}_{\parallel}^2 \rangle$  and  $\langle \sigma_{\parallel}^2 \rangle$ . In practice our averages must be confined to some inner region and we must investigate the seriousness of the error incurred by this confinement. The final problem is how to determine the required ratio  $W_{zz}/W_{xx}$  of components of the potential-energy tensor. In principle this may be done from the photometry (e.g. Binney & Strimpele 1978). A much simpler alternative is to assume that the isodensity surfaces have a constant ellipticity  $\epsilon$ , which allows  $W_{zz}/W_{xx}$  to be determined independently of the radial density profile. In most of the tests below I have used this crude approach, with  $\epsilon$  taken to be a weighted average  $\bar{\epsilon}$  of the ellipticities of individual isophotes. After some experimentation, the weighting scheme adopted was

$$\bar{\epsilon} = \frac{\int dR R^2 \Sigma(R, 0) \epsilon(R)}{\int dR R^2 \Sigma(R, 0)}, \quad (29)$$

where  $\Sigma(R, 0)$  denotes the surface brightness distance  $R$  down the apparent major axis.

Insight into the uncertainties that will be encountered when using real data is provided by applying equation (28) to pseudo-data obtained by projecting Evans and Rowley models.

The upper panel of Fig. 3 shows the projected rotation rate and ellipticity of an Evans model with  $y = 0.25$  and  $q_{\Phi} = 0.9$ .<sup>1</sup> Because the rotation curve rises very steeply near the centre (in three dimensions  $\bar{v}$  does not tend to zero as the origin is approached),  $\alpha \approx 0.2$  is relatively large: the

<sup>1</sup> The final integral in the definition of  $W_{ij}$  diverges for Evans models with  $y < 0.25$ .

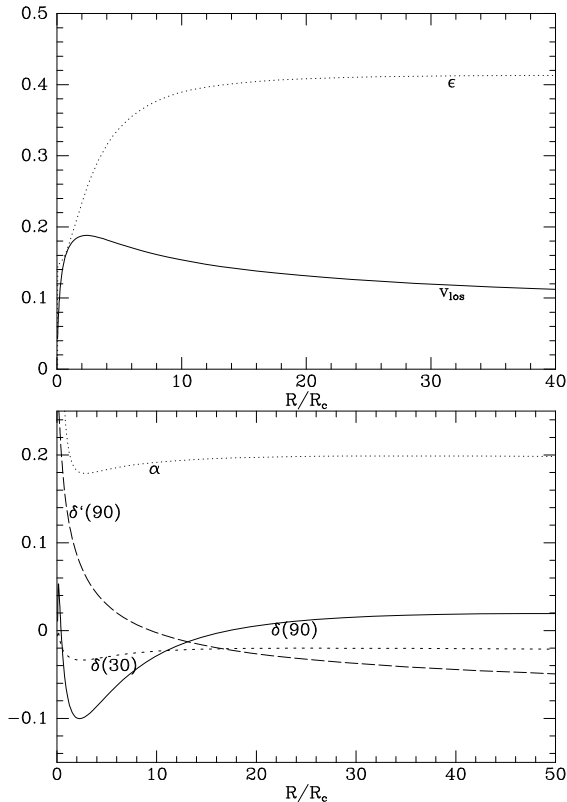


**Figure 3.** Upper panel: projected rotation speed and ellipticity for an Evans model. Lower panel: the parameter  $\alpha$  defined by equation (27) (dotted curve) and the global anisotropy parameter  $\delta$  estimated from equation (28) using only data from within the circle of radius  $R$ ; at edge-on orientation (full curve) and for inclination  $i = 30^\circ$  (short-dashed curve). The long-dashed curve shows values of  $\delta$  recovered at edge-on orientation when the true ratio  $W_{zz}/W_{xx}$  is used in (28) instead of an estimate based on the assumption that all isodensity surfaces are similar spheroids.

dotted curve in the lower panel of Fig. 3 shows as a function of radius  $R$  the value of  $\alpha$  obtained by carrying the integrals involved in its definition (27) only out to  $R$ . The full curve in the lower panel shows as a function of  $R$  the values of  $\delta$  yielded by equation (28) when the model is seen edge-on and  $W_{zz}/W_{xx}$  is evaluated under the assumption of constant ellipticity,  $\bar{\epsilon}$ . Small positive values of  $\delta < 0.075$  are obtained, and outside the core (where  $\alpha$  becomes large)  $\delta$  rises slowly with  $R$  because  $\epsilon$  is rising, while the streaming velocity is very nearly constant. The long-dashed curve shows the values of  $\delta$  obtained when  $W_{zz}/W_{xx}$  is set equal to the value it assumes at large radii. The decline of this curve reflects the outward-increasing nature of  $\epsilon$ . The fact that at  $R \simeq 50R_c$  this curve has fallen to small negative  $\delta \simeq -0.05$  suggests that the procedure intended to make the model an isotropic rotator was not wholly successful. The offset between the end points of the full and long-dashed curves gives an indication of the error in  $\delta$  that is inherent in adopting a constant ellipticity.

Fig. 4 shows equivalent data for the Rowley model that has  $\Delta = 4$  and  $\omega r_a/\sigma = 1.69$ . Because this model has a substantial region of near solid-body rotation,  $\alpha \lesssim 0.03$  is much smaller than in the case of the Evans model. When the model

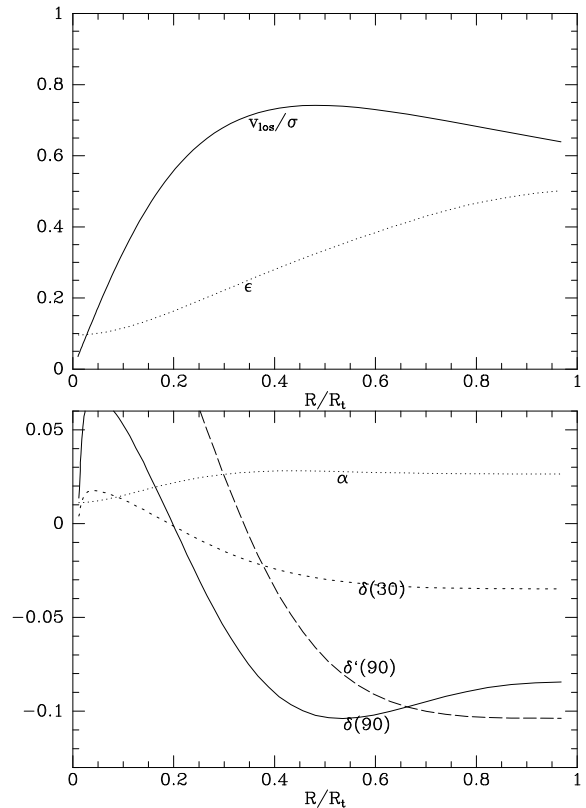


**Figure 4.** As Fig. 3 but for a Rowley model.

is viewed edge-on,  $\delta$  falls by  $0.35R_t$  to  $\delta = -0.075$  and from there to the edge of the model oscillates in a small range around  $-0.097$ . The end-point of the long-dashed curve, which is based on the exact ratio  $W_{zz}/W_{xx}$ , lies within this range because at most radii the azimuthal velocity dispersion is smaller than the other two principal dispersions.

The short-dashed curves in the lower panels of Figs 3 and 4 show that remarkably small values of  $\delta$  are obtained when equation (28) is applied to data obtained from the models at inclination  $i = 30^\circ$ . Since equation (28) was derived for edge-on inclination, we have no guarantee that a realistic value of  $\delta$  will be obtained at small inclinations. Moreover, in Fig. 1 both models move away from the isotropic-rotator line towards negative  $\delta$  as the inclination is reduced. Hence it comes as a pleasant surprise to find that equation (28) works well at small inclinations.

## 5 CONCLUSIONS

The degree of anisotropy in the velocity distribution of an elliptical galaxy is probably an important clue to the manner in which the galaxy formed. Traditionally anisotropy has been estimated from the ratio  $v_{\text{max}}/\sigma_{0.5}$  of the maximum measured rotation velocity to a central mean of the velocity dispersion. By a distinctly ad-hoc scaling, the tensor virial theorem has been used to draw a curve on the  $(v/\sigma, \epsilon)$  plane for isotropic rotators, and galaxies that lie significantly below this curve have been deemed to have anisotropic velocity distributions. Fig. 1 validates this procedure by showing

the models with nearly isotropic velocity distributions are placed near the curve of isotropic rotators.

A much more rigorous procedure is possible now that one can map rotation speed and velocity dispersion over a substantial fraction of a galaxy's image. One replaces  $v_{\max}/\sigma_{0.5}$  with the ratio  $\langle \tilde{v}_{\parallel}^2 \rangle / \langle \sigma_{\parallel}^2 \rangle$  of the sky-averaged squared rotation velocity to the squared velocity dispersion. Equation (26) rigorously relates this average to the global anisotropy parameter  $\delta$ , a shape-dependent ratio of potential-energy tensor components, and the dimensionless quantity  $\alpha$  that measures the degree of shear in the stellar streaming velocity. Alternatively, equation (28) expresses the anisotropy parameter as a function of quantities that are either directly observable ( $\langle \tilde{v}_{\parallel}^2 \rangle / \langle \sigma_{\parallel}^2 \rangle$  and  $W_{zz}/W_{xx}$ ) or can be estimated to sufficient accuracy from the data ( $\alpha$ ).

An obvious problem with the rigorous approach is that the sky-averages that appear in the TVT extend over the whole image, while data are available only within some limiting radius  $R$ . Figs 3 and 4 suggest that  $\delta$  can be estimated to an uncertainty  $\simeq 0.05$  from data that extend out to  $\gtrsim 15R_c$  in a galaxy that resembles an Evans model (in which the ellipticity reaches a plateau around  $10R_c$ ), or  $\gtrsim 0.35R_t$  in a galaxy like a Rowley model (in which  $\epsilon$  roughly linearly to the edge of the system). It is unfortunate that when we confine ourselves to semi-analytic models, we are able to investigate the impact of restricted sky coverage only with models that have  $\delta \simeq 0$ . Tests on systems with  $\delta \gg 0$  could be carried out with N-body models.

Traditionally, anisotropy has been quantified as the ratio  $(v/\sigma)^*$  of the measured quantity  $v_{\max}/\sigma_{0.5}$  to the height of the isotropic-rotator curve at a value of  $\epsilon$  that is characteristic of the galaxy. This work suggests that anisotropy can in future be more rigorously quantified by the anisotropy parameter  $\delta$ .

## REFERENCES

- Aarseth S.J., Binney J.J., 1978, MNRAS, 185, 227  
 Bacon R. et al. 2002, in *Scientific Drivers for ESO Future VLT/VLTI Instrumentation*, eds J. Bergeron, G. Monnet, Springer, Berlin, p. 108  
 Barnes J.E., Hernquist L., 1992, ARA&A, 30, 705  
 Bender R., 1988, A&A, 193, L7  
 Bertola F. & Capaccioli M., 1977, ApJ, 211, 697  
 Binney J., 1976, MNRAS, 177, 19  
 Binney J., 1978, MNRAS, 183, 501  
 Binney J., Strimpel O., 1978, MNRAS, 185, 473  
 Binney J., Tremaine S., 1987, 'Galactic Dynamics', Princeton NJ: Princeton University Press  
 Chandrasekhar S., 1969, 'Ellipsoidal Figures of Equilibrium', New Haven Conn: Yale University Press  
 de Zeeuw P.T. et al., 2002, MNRAS, 329, 513  
 Davies R.L., Efsthathiou G., Fall S.M., Illingworth G. & Schechter P.L., 1983, ApJ, 266, 41  
 Evans N.W., 1994 MNRAS, 267, 333  
 Hernquist L., 1990, ApJ, 356, 359  
 Illingworth G., 1977, ApJ, 218, L43  
 Jaffe W., 1983, MNRAS, 202, 995  
 Kelz A., Roth M.M., Becker T., 2003, SPIE, 4841, 1057  
 King I.R., 1966, ApJ, 71, 64  
 Kormendy J., Bender R., 1996, ApJ, 464, L19  
 Levison H.F., Richstone D.O., 1985, ApJ., 229, 349  
 Naab T., Burkert A., 2003, ApJ, 597, 893  
 Naab T., Burkert A., Hernquist L., 1999, ApJ, 523, L133  
 Roberts P.H. 1962, ApJ, 136, 1108  
 Rowley G., 1988, ApJ, 331, 124  
 Schwarzschild M., 1979, ApJ., 232, 236